2022 13th International Symposium on Communication Systems, Networks and Digital Signal Processing (CSNDSP) | 978-1-6654-1044-1/22/$31.00 ©2022 IEEE | DOI: 10.1109/CSNDSP54353.2022.9907908

Design and Experimental Evaluation of a Bluetooth 5.1 Antenna Array for Angle-of-Arrival Estimation

Nuno Paulino and Luís M. Pessoa
INESC TEC and Faculty of Engineering,
University of Porto, Porto, PORTUGAL
{nuno.m.paulino, luis.m.pessoa}@inesctec.pt

André Branquinho and Edgar Gonçalves
Wavecom – Soluções Rádio SA,
Aveiro, PORTUGAL
{abranquinho, egoncalves}@wavecom.pt

***Abstract*—One the of the applications in the realm of the Internet-of-Things (IoT) is real-time localization of assets in specific application environments where satellite based global positioning is unviable. Numerous approaches for localization relying on wireless sensor mesh systems have been evaluated, but the recent Bluetooth Low Energy (BLE) 5.1 direction finding features based on Angle-of-Arrival (AoA) promise a low-cost solution for this application. In this paper, we present an implementation of a BLE 5.1 based circular antenna array, and perform two experimental evaluations over the quality of the retrieved data sampled from the array. Specifically, we retrieve samples of the phase value of the Constant Tone Extension which enables the direction finding functionalities through calculation of phase differences between antenna pairs. We evaluate the quality of the sampled phase data in an anechoic chamber, and in a real-world environment using a setup composed of four BLE beacons.**

***Index Terms*—BLE, Bluetooth, wireless sensor networks, mesh networks, Angle-of-Arrival, signal processing, Internet-of-Things**

I. Introduction

The push towards the long promise of the IoT is gaining momentum as more efficient telecommunications are implemented, concurrently with increasingly more feature-full System-on-Chip (SoC) solutions. Together, these advances are powering more ambitious edge computing applications. One such application is real-time localization of devices or assets in context-specific indoor spaces [1].

Towards this, direction finding capabilities have been recently added to the Bluetooth Specification, as of version 5.1 [2]. Specifically, direction finding is performed by sampling a Constant Tone Extension (CTE) which is appended to the end of a Bluetooth packet. A Radio Frequency (RF) device with an array of antennas, can sample the phase of this tone at each of the antennas, and derive the AoA of the signal via the phase differences between antennas. Specific details of the processing depend on the number of antennas and their physical arrangement.

In this paper, we consider an application context where mobile BLE receivers are equipped with an antenna array, envisioning application scenarios for self-localization of vehicles in warehouses, shipping ports, or similar environments. In these scenarios, the number of receivers wishing to know their location is known, and potentially small. So this allows for the installation of fixed, cheap BLE beacons in legacy locations which may not have the wall-power and ethernet infrastructure required by the opposite solution, i.e., when the arrays are fixed and numerous, and the number of assets to locate is unknown and have only one antenna (e.g., exhibition halls or shopping malls).

In previous work, we performed a simulation based evaluation for positioning and tracking [3], based on this topology, as a function of the number of beacons, receiver movement, among others. As the receiver moves, fast computation is required, as well as a reduced number of packets per fixed transmitter, to compute a position. We demonstrated that AoA data received by multiple transmitters can allow the receiver to compute its own position. However, computing the AoA requires prior signal processing over the previously mentioned phase samples. Therefore, if possible, computational complexity should be reduced in order to achive this in real-time on such edge devices.

In this paper, we focus on obtaining and processing the CTE phase samples, and evaluating the quality of the obtained data in a real-world scenario, by designing and implementing a Printed Circuit Board (PCB) with a circular antenna array with 8 antennas. We present the theoretical expected behaviour using generated phase data, verify the correct operation of the design in an anechoic chamber, and finally evaluate the quality of the data attainable in an outdoor environment free of obstructions.

II. Related Work

Two data processing steps are proposed in [4], in order to improve AoA estimations from raw phase data, including a comparison with the state-of-the-art algorithm Multiple Signal Classification (MUSIC) [5]. Using one commercial transmitter and one commercial linear array, the authors retrieve 200 packets per orientation between the two devices in steps of $10°$ in the range of $-90°$ to $90°$ (the range the linear receiver is capable of disambiguating). The devices are $1\,\mathrm{m}$ off the ground and $2\,\mathrm{m}$ apart in an indoor location. The first data processing step, a non-linear recursive least square method, intends to mitigate the effect of multi-path and noise. A second step employs an unscented Kalman filter to reduce the effect of different oscillator frequencies between transmitter and receiver

This work is financed by the ERDF - European Regional Development Fund through the Norte Portugal Regional Operational Programme - NORTE 2020 under the Portugal 2020 Partnership Agreement within project DECARBONIZE, with reference NORTE-01-0145-FEDER-000065.

(introduced to account for manufacture variation). For the described setup, the pre-processing leads to a decrease in the computed AoA of $3.8°$ on average, although at the cost of increased computational load.

Similarly, comparable pre-processing steps are applied to the raw In-Phase/Quadrature (I/Q) samples in [6]. Namely, a non-linear least square curve fitting method to reduce the effect of noise on the I/Q samples, a Kalman filter to address frequency and phase offsets inherent to the different antennas in the array and the switching process. A third step is added relative to [4], where a Gaussian filter compensates for estimation errors which are introduced depending on which BLE data channel is being used, as the approach assumes a connected mode. For one commercial transmitter and receiver pair, with a linear array with 3 elements, placed $1\,\mathrm{m}$ apart in an unspecified test environment, the approach reduces the estimation error significantly in the range of $-60°$ to $60°$. As with [4], AoA estimation for linear arrays significantly decays when the incident angle is parallel to the array.

In [7] the BLE 5.1 direction-finding is implemented via Software Defined Radio (SDR) on a Xilinx Zynq-7000 System-on-Chip. The authors design their own linear array with 4 rectangular patch microstrip antennas, and employ a commercial radio module and RF switch. A single BLE beacon is placed $3\,\mathrm{m}$ away from the receiver setup, and the beacon is moved along the azimuth plane (parallel to the forward face of the antenna array), for a range of $-90°$ to $90°$. Resorting to the MUSIC algorithm, the design achieves a root mean square error up to $5°$.

III. Proposed Approach

Regarding the design of the antenna array, as Section II mentions, arrays are typically either linear or circular. Linear arrays are easier to implement, but suffer from ambiguity regarding the true AoA, while circular arrays offer data redundancy due to inherent symmetry [8]. Therefore, although circular array designs are not novel, they are still actively used and studied for direction finding applications [9], [10]. Due to the recent direction finding features added to BLE, they are now being explored for use in combination with this protocol.

In this paper, we evaluate a BLE based localization approach using our own design and software for a circular antenna array with 8 antennas. The following sections explain the physical design of the board, the signal processing involved, and the theoretical expected behaviour.

A. Design of Circular 8-Antenna Array

We have designed and fabricated a circular printed circuit board equipped with a single Nordic Semiconductor nRF52811 micro-controller [11]. This micro-controller supports the direction finding features specified by BLE 5.1 [2].

The board is $13\,\mathrm{cm}$ in diameter, and its 8 antennas are equally spaced, i.e., placed at $45°$ steps relative to the center of the board. At the center, the board contains at SKY13418-485LF switch [12], which is a SP8T RF switch rated up to $6\,\mathrm{GHz}$. The tracks from the switch to each SMA connector have equal lengths. Besides these components, the board contains a 10-pin header, used for programming the micro-controller via an external devkit [13], via a J-Link interface, and also to serve as the serial interface for data transfer from the antenna array board to a workstation. A micro-USB connector is used only for power, with a $5\,\mathrm{V}$ to $2.5\,\mathrm{V}$ regulator [14]. This regulator supplies both the radio switch, and the micro-controller. The board was fabricated in an FR-4 substrate with a thickness of $1\,\mathrm{mm}$.

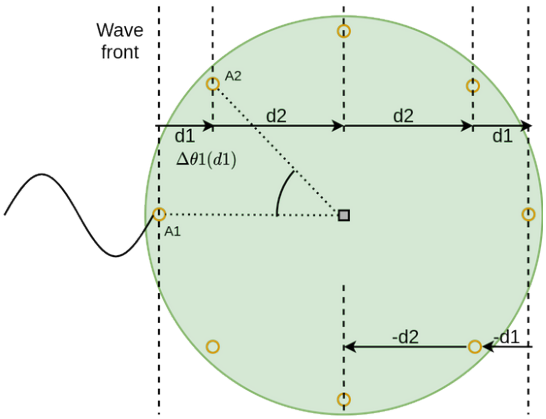

Fig. 1. Model of circular antenna array, and relationship between angle, and travelled distance between antenna pairs

The micro-controller is programmed in *C*, and we rely on Nordic's own software development kit to configure the radio parameters for both the receiver and transmitter software versions. On the receiver, control of the RF switch is done via three control pins between the micro-controller and the switch. During reception of a packet, the micro-controller's follows a preset switching pattern (configured at boot), which repeats, to select one antenna per switching period. During sampling, a data array in memory is directly filled with all received samples by the nrRF52811's integrated radio. The radio is capable of providing the phase samples both in I/Q format or magnitude-phase format. We employ the latter format, and process the phase values given directly by the radio. Each sample is represented in a $[-201, 201]$ fixed-point value range, stored in a $16\,\mathrm{bit}$ integer. We currently transmit all phase samples to a workstation and compute the phase differences, and do not currently use the magnitude value.

Figure 1 illustrates the simplified board design (tracks omitted), and how sampling multiple antennas in the array, in a known pattern, allows for determination of the incident AoA by the receiver itself in a $360°$ range. Antennas are numbered sequentially clockwise. As with linear arrays, the distance travelled by the incident electromagnetic plane wave front between neighbouring antennas depends on the incident angle. For a circular array, this implies a symmetry in the phase differences between certain antenna pairs. For example, the same phase differences will be observed between antennas A2 and A3, and A3 and A4, as the same distance *d2* is travelled by the wave front, as shown in the following section.

B. Phase Difference Calculation

The BLE 5.1 specification for a direction-finding enabled packet states that the CTE portion begins with a $4\,\mu s$ guard period, followed by a $8\,\mu s$ reference period, during which one antenna set as reference is sampled at a higher rate, before the switching pattern begins. The reference samples can be used to predict the phase values at subsequent timesteps, during which the following antennas are sampled [15].

However, we do not utilize the reference samples, and directly compute the phase differences by using the samples retrieved in sequence, from two neighbour antennas. As our switching period is set to $4\,\mu s$, and since the $250\,kHz$ frequency of the CTE implies that the phase varies 90º per $1\,\mu s$, then each *i-th* phase sample from an antenna will have an equivalent value after $4\,\mu s$.

Therefore, we take all the samples from all antennas, and first apply an unwrapping step to the phase values, shown in Algorithm 1. This is required since, although the phase progresses linearly, its reported value is bound to the $[-201, 201]$ range given by the nRF52811's radio. We convert this fixed-point representation to floating-point within the more easily interpretable $[-180, 180]$ range.

Algorithm 1: Algorithm to unwrap the *j* phase samples from each *i-th* antenna from the $[-180, 180]$ bound

```
nrSampleGroups ← 32;
nrSamples ← 3;
for i < nrSampleGroups do
    for j < nrSamples do
        if sample_ij < sample_ij−1 − 180 then
            k ← j;
            for k < nrSamples do
                sample_ik = sample_ik + 360;
            end
        end
    end
end
```

To compute each of the $n = 0, ..., N$ phase differences, we take the $i = 0, ..., S$ samples from each pair of neighbour antennas, subtract each *i-th* sample pair, and take the mean of the differences as the phase difference for that antenna pair. Finally, we compute the modulus to bind the value to a $-180°$ to $180°$ range, as per Algorithm 2. In this case $N = 32$, and $S = 2$. We utilized only 3 out of the 8 samples per antenna as a result of previous experiments in the anechoic chamber (omitted for brevity), where we observed that 5 out of the 8 samples were too unreliable. We retain the second to fourth samples, as the remaining are affected by the switching behaviour of the RF switch.

C. Expected Behaviour

Knowing the geometry of the board, the physical placement of its antennas, the frequency of the CTE, and the sampling parameters, we can generate simulated phase sample data. The purpose of this is to validate the algorithms for phase difference calculation in an ideal case, unaffected by potential design flaws of the board, or ambient conditions, which would compromise any further calculations.

Algorithm 2: Calculation of phase difference between antenna pairs

```
diffs[32] ← 0; //32 phase differences
nrSampleGroups ← 32;
nrSamples ← 3;
for i < nrSampleGroups do
    d[nrSamples] ← 0;
    for j < nrSamples do
        d[j] = sample_i−1,j − sample_i,j;
    end
    diffs[i] = mod(mean(d) + 180, 360) − 180;
end
```

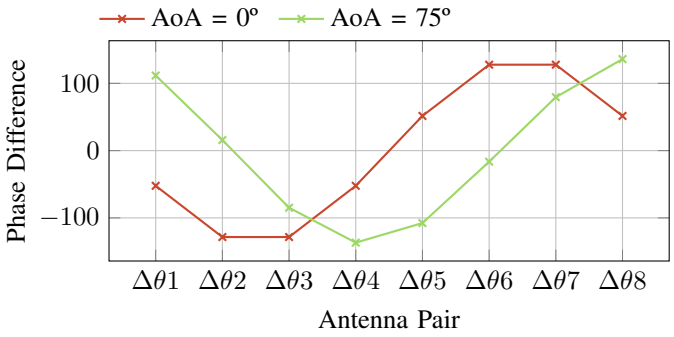

Fig. 2. Profile of calculated phase difference values for all adjacent antenna pairs, as a function of two different AoAs, using phase sample data generated according to the mode (e.g., pair 1 is the difference between the phase value between A1 and A2 ($\Delta\theta 1$), at the same instant in time)

Figure 2 illustrates the eight phase differences, for the eight antenna pairs, generated by processing generated phase data for two incident angles (as data is generated, the exact AoA is illustrative and not related to the board design). Due to the board's geometry, the resulting profile of the phase differences is itself a sinusoidal wave, whose own phase shifts as a function of the AoA. Therefore, determining this phase, e.g., via curve fitting, would be a subsequent step to arrive at an AoA.

The resulting phase difference profile is in practice affected by noise, which originates from multi-path effects, differences in oscillators between transmiters and receivers, behaviour of the RF switch, or even slight variations in impedances of the antenna tracks or physical separation between antenna pairs. To illustrate this, we introduce gaussian noise to the phase samples we generate via simulation, and Figure 3 demonstrates the degradation of the profile based on noise with zero mean, and the shown standard deviation (σ).

D. Position Calculation from Multiple Angles-of-Arrival

In this paper, we do not yet advance into location calculation, and focus on the quality of the attained phase data in the

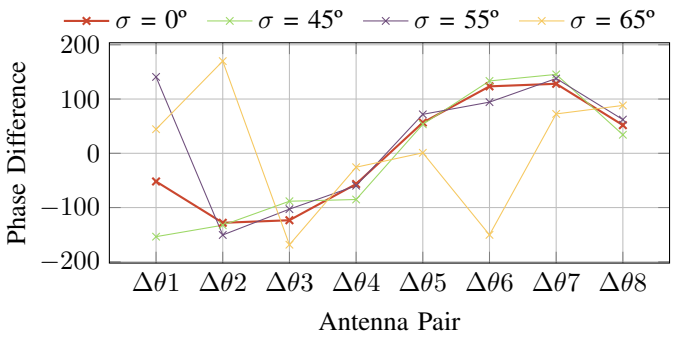

Fig. 3. Effect of guassian error with zero mean ($\mu = 0$) and for different standard deviations (σ)

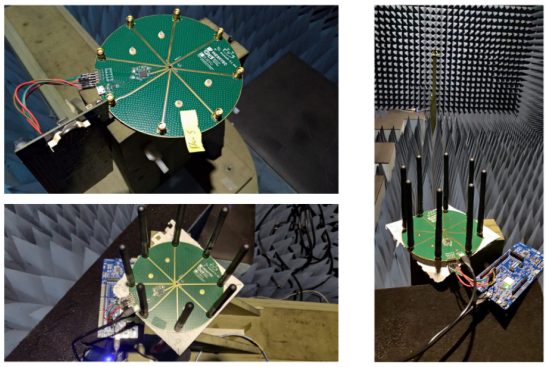

Fig. 4. Fabricated board design, and setup for retrieval of packets in anechoic chamber

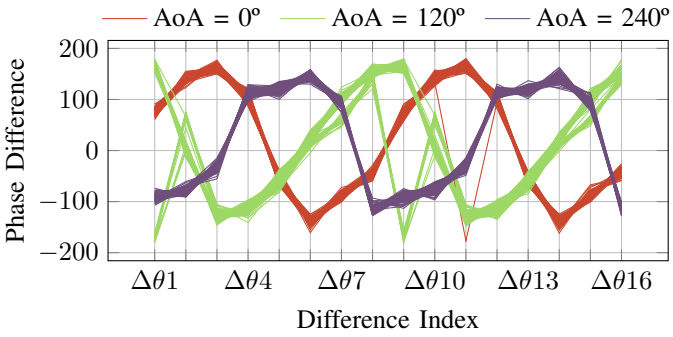

Fig. 5. Superposition of phase difference profiles for 3 incident angles, for a total of 100 packets retrieved in anechoic chamber, per angle. A consistent profile is observed, using the calculation methods explained.

presented experimental environment. However, we will shortly explain the method we previously validated in [3].

We target application scenarios where a mobile receiver wishes to self locate. Therefore, by relying on knowledge of the map, and on the absolute position fixed position of the beacons, multiple AoAs would generate vectors that, in ideal conditions, would intersect in a single point. In such a case, even two AoAs would be sufficient for receiver localization. However, due to noise present in the CTE phase samples, an intersection between two vectors alone could lead to a significant positioning error. Position calculation improves with more AoAs from different source beacons. Even so, we can only compute a candidate area, i.e., polygon, for the position of the receiver. We thus resort to state-of-the-art least-squares method which computes a point whose total distance to each side of the polygon is smallest [3], [16].

IV. Experimental Evaluation

Using a total of five boards, we conducted two experimental evaluations. In both cases, one board was used as a receiver, while the remaining four were programmed as transmitters. The transmitter code, past the configuration portion, is a simple loop which broadcasts a direction-finding enabled packet where the payload is the transmitter's unique ID. The transmission power was set to $4\,\mathrm{dBm}$.

For all tests, we configured the CTE length to $160\,\mu\mathrm{s}$, the switching period to $4\,\mu\mathrm{s}$, and the sample rate to $500\,\mathrm{ns}$. This means that each BLE packet produces 304 samples of it's constant tone's phase, 8 per sampled antenna. The sampling pattern is circular, meaning sampling starts from antenna 1, and follows the board perimeter. Since the switching pattern repeats, the full perimeter of the board is sampled multiple times during the CTE. Specifically, four sampling rotations are performed, leading to 32 phase differences.

Firstly, we validated the expected behaviour of the receiver in an anechoic chamber, and secondly, we evaluated the quality of the received data in a field test.

A. Phase Data Gathering in Anechoic Chamber

Figure 4 shows an experimental setup in an anechoic chamber. A single transmitter is placed in a static support, while the receiver is placed in a rotating mount. We rotate the receiver in steps of $15°$, and gather one hundred packets per orientation. The distance between the transmitter and receiver is approximately $5\,\mathrm{m}$.

For all retrieved packets per orientation, we computed the respective phase difference profiles, using the total of 104 samples retrieved per packet, arriving at the 32 differences between neighbouring antennas. Figure 5 illustrates this for 100 packets and 3 different orientations, demonstrating that the sampled phase data and phase differences follow the expected behaviour.

B. Phase Data Gathering in Field Test

A field test was conducted with four boards programmed as transmitters, with only one antenna, and one board programmed as receiver, making use of the entire 8-antenna array.

The outdoor location was a flat, concrete floored lot, without obstructions. The aerial view is illustrated in Figure 6a. The total area of the lot is approximately $1.5\,\mathrm{km}^2$, however, we utilized a sub-section of this area for the experiments. The area outlined in red is a square with a side of $12\,\mathrm{m}$ in length. At each corner, we placed one of the transmitters, and for each grid location within the area, we placed the receiver, until a total of 600 packets were received for that location. The

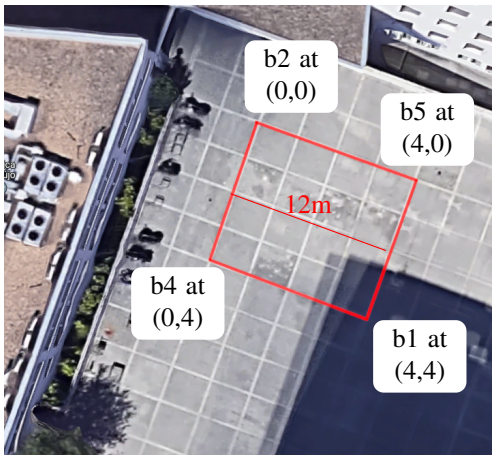

(a) Aerial view of the field test location: an unobstructed space with a rugged concrete floor at the Faculty of Engineering of the University of Porto

(b) Receiver placed along one of the edges of the outlined space, with laptop arrangement to store received BLE packet phase data from all four transmitters.

Fig. 6. Aerial view of test location (Figure 6a), and retrieval of data for one possible receiver position (Figure 6b)

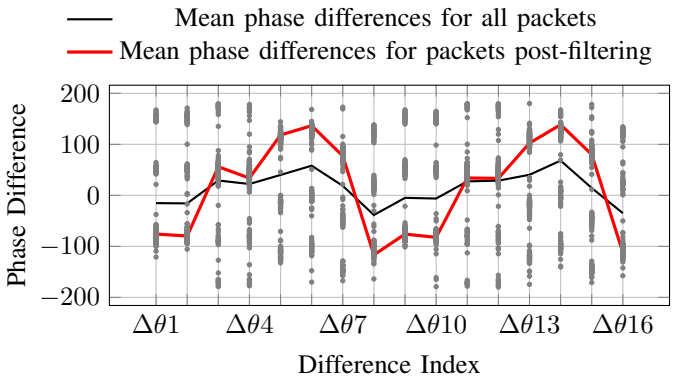

Fig. 7. Superposition of all computed phase differences (in light gray) for all received packets sent by board #2 (a total of 170) at the center of the test area (x=2, y=2). The average of all profiles is shown in black. Despite the variation between packets, the sinusoidal behaviour of the phase difference profile is observable. However, taking only the most frequently ocurring value for each $\Delta\theta$, a much clearer profile is achievable, shown in red.

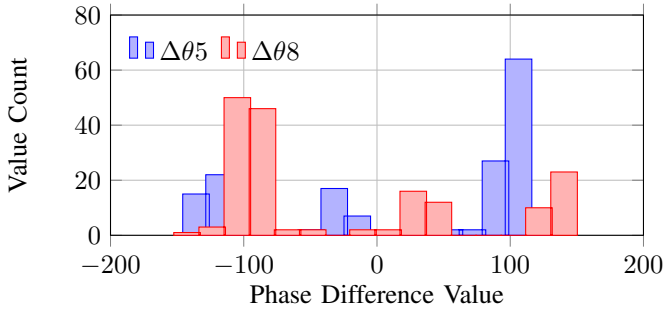

Fig. 8. Two example histograms (for 16 bins) of the values of the measured phase differences for $\Delta\theta5$ and $\Delta\theta8$, demonstrating the more frequent occurrence of the phase difference values.

receiver faced the same absolute direction for every placement. Figure 6b shows this described setup, with the receiver placed along on of the edges of the outlined area. The boards are held on tripods, parallel to and approximately $1.6\,\mathrm{m}$ off the ground. All the transmitters use the same respective antenna track for transmission.

The purpose of gathering a large number of packets per transmitter, per location of the map, was to validate the expected behaviour, in a real-world setting. That is, we expected that, for a given transmitter and receiver pair, that all the packets from that transmitter, when processed, would produce phase difference profiles similar to those shown in Figure 5.

For brevity and clarity, we show these results for the central position of the map, only for the packets sent by board #2, which is located at the lower right corner of the area shown in Figure 6a, from which a total of 170 packets were received. Figure 7 illustrates, in light grey marks, the phase difference values between antenna pairs, e.g., $\Delta\theta1$.

The average phase difference profile is shown in black. The expected sinusoidal profile is observed, although, unlike the coherent behaviour observed in the anechoic chamber, the resulting profile is degraded. However, it is noticeable that, per phase difference, there are multiple clusters of points. For example, for $\Delta\theta1$, there are three noticeable groups of points. Each group represents one possible value for the phase difference $\Delta\theta1$.

Given this, we compute one histogram per phase difference value, and determine the most frequently occurring value for that difference. This results in the average phase difference profile shown in red in Figure 7. Figure 8 illustrates this for two of the phase difference values. The x axis shows the possible values for the phase difference, while the y axis shows the counts for the value ranges within the 16 bins. For both examples, there is an observable higher count for two values, while two other frequent values occur, at much lower counts.

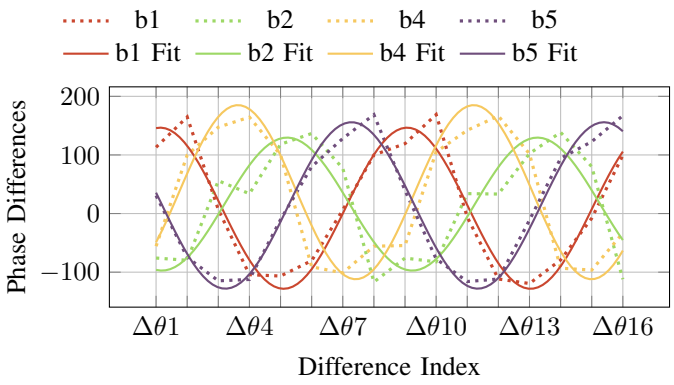

Fig. 9. Phase difference profiles between the receiver, place at the center of the test area, and all beacons. In dotted lines we show the phase differences after histogram based filtering, and in solid lines a sinusoidal fit. The four waves display phase differences of 90°, e.g., between *b1* and *b4*, which is the expected behaviour given the physical disposition of the boards

Finally, we can demonstrate the relationship between the horizontal displacement of the phase difference profile and the AoA, as shown in Figure 9. By placing the receiver at the center of the map (always with the same absolute orientation), the AoAs received from any two neighbouring beacons (e.g., *b1* and *b5*) will be offset by plus or minus 90°. By defining one specifc phase difference profile as a reference for the receiver's relative 0°, we can attain the AoA by determining the displacement relative to that reference.

V. Conclusion

This paper has presented a design of a circular 8-antenna array, with the intent of designing a self-localizing receiver. We briefly explained the methodology of phase difference calculation between neighbouring antenna pairs, and how the eight differences can be combined to estimate an AoA.

We have demonstrated the effect that noise in the raw phase measurements can produce in the phase difference profile via simulation, and conducted two experimental evaluations. The first demonstrated the correct behaviour of the design versus the theoretical model in an anechoic chamber, as a function of the relative orientation of the receiver and transmitter. The second was a field test using four transmitters placed at the vertices of a 12 m by 12 m area. Although it is possible to extract the expected phase difference profiles, the receiver must remain still at the same location, so that the effects of noise can be averaged out by reception of multiple packets. Regarding pre-processing, we have also briefly demonstrated how reflections may be filtered out and attain the desired behaviour. We will attempt to explore this further, by resorting to the currently unused magnitude values and the best known location of the receiver itself.

In order to allow for the capability of self-localization on this kind of embedded device with limited computing power, subject to movement and relying on the small number of packets, as we have previously evaluated [3], requires further study, as computationally demanding algorithms may compromise how quickly a position can be computed, especially since multiple AoAs are required.

As it is difficult to reduce the error from the obtained phase measurements themselves, future work will focus on extracting more robust phase differences despite this noise. We plan to evaluate the viability of machine learning models to extract the AoA from phase difference data, as some recent approaches are attempting [17], [18], especially to reduce the computational cost of the existing algorithms [5].

References

[1] F. Zafari, A. Gkelias, and K. K. Leung, "A survey of indoor localization systems and technologies," *IEEE Communications Surveys Tutorials*, vol. 21, no. 3, pp. 2568–2599, 2019.

[2] Bluetooth SIG. (2019) Bluetooth Specification Version 5.1. [Online]. Available: https://www.bluetooth.com/bluetooth-resources/bluetooth-core-specification-v5-1-feature-overview/

[3] N. Paulino, L. M. Pessoa, A. Branquinho, and E. Gonçalves, "Evaluating a Novel Bluetooth 5.1 AoA Approach for Low-Cost Indoor Vehicle Tracking via Simulation," in *2021 Joint European Conf. on Networks and Communications 6G Summit (EuCNC/6G Summit)*, 2021, pp. 259–264.

[4] S. He, H. Long, and W. Zhang, "Multi-antenna array-based aoa estimation using bluetooth low energy for indoor positioning," in *2021 7th Intl. Conf. on Computer and Communications (ICCC)*, 2021, pp. 2160–2164.

[5] R. Schmidt, "Multiple emitter location and signal parameter estimation," *IEEE Transactions on Antennas and Propagation*, vol. 34, no. 3, pp. 276–280, 1986.

[6] Z. Hajiakhondi-Meybodi, M. Salimibeni, K. N. Plataniotis, and A. Mohammadi, "Bluetooth low energy-based angle of arrival estimation via switch antenna array for indoor localization," in *2020 IEEE 23rd Intl. Conf. on Information Fusion (FUSION)*, 2020, pp. 1–6.

[7] F. A. Toasa, L. Tello-Oquendo, C. R. Peñafiel-Ojeda, and G. Cuzco, "Experimental demonstration for indoor localization based on aoa of bluetooth 5.1 using software defined radio," in *2021 IEEE 18th Annual Consumer Communications Networking Conf. (CCNC)*, 2021, pp. 1–4.

[8] C. Usha Padmini and P. S. Naidu, "Circular array and estimation of direction of arrival of a broadband source," *Signal Processing*, vol. 37, no. 2, pp. 243–254, 1994. [Online]. Available: https://www.sciencedirect.com/science/article/pii/0165168494901066

[9] S. V. Ballandovich, Y. G. Antonov, G. A. Kostikov, L. M. Liubina, and M. I. Sugak, "Development of the ultra-wideband circular antenna array," in *2020 Systems of Signal Synchronization, Generating and Processing in Telecommunications (SYNCHROINFO)*, 2020, pp. 1–4.

[10] A. V. S. Swathi, V. V. S. S. S. Chakravarthy, and M. V. Krishna, "Circular antenna array optimization using modified social group optimization algorithm," *Soft Comput.*, vol. 25, no. 15, p. 10467–10475, aug 2021.

[11] N. Semiconductor. (2021) nRF52811 Product Specification v1.1. [Online]. Available: https://infocenter.nordicsemi.com/pdf/nRF52811_PS_v1.1.pdf

[12] Skyworks. (2019) SKY13418-485LF 0.1-6.0 GHz SP8T Antenna Switch. [Online]. Available: https://www.skyworksinc.com/Products/Switches/SKY13418-485LF

[13] N. Semiconductor. (2018) nRF52840 Development Kit. [Online]. Available: https://infocenter.nordicsemi.com/pdf/nRF52832_PS_v1.4.pdf

[14] T. Instruments. (2001) TPS76925. [Online]. Available: https://www.ti.com/lit/ds/symlink/tps769.pdf

[15] M. Cominelli, P. Patras, and F. Gringoli, "Dead on Arrival: An Empirical Study of the Bluetooth 5.1 Positioning System," in *Proc. of the 13th Intl. Workshop on Wireless Network Testbeds, Experimental Evaluation & Characterization*, 2019, pp. 13–20.

[16] J. Traa, "Least-squares Intersection of Lines," University of Illinois Urbana-Champaign (UIUC), 2013.

[17] A. Khan, S. Wang, and Z. Zhu, "Angle-of-arrival estimation using an adaptive machine learning framework," *IEEE Communications Letters*, vol. 23, no. 2, pp. 294–297, 2019.

[18] M. Yang, B. Ai, R. He, C. Huang, Z. Ma, Z. Zhong, J. Wang, L. Pei, Y. Li, and J. Li, "Machine-learning-based fast angle-of-arrival recognition for vehicular communications," *IEEE Transactions on Vehicular Technology*, vol. 70, no. 2, pp. 1592–1605, 2021.